A 3-Channel Inductive Angular Position Sensor Interface with Harmonic Suppression Achieving 0.072° Measurement Error and 1.48 μs Latency

Yiming Wang[1], Tianxiang Qu[1], Xiaofa Yang[2], Jianyu Zhu[2], Kaiwen Zhou[1], Zhiliang Hong[1] and Jiawei Xu[1]
[1]Fudan University, Shanghai, China. [2]Novosense Microelectronics, Shanghai, China
Email: jwxu@fudan.edu.cn

***Abstract*—This paper presents a high-accuracy 3-channel inductive angular position sensor (IAPS) interface for precise motor speed monitoring with enhanced harmonic suppression and low-latency signal processing. The proposed architecture includes phase-compensated transmission (TX) and receiving (RX) channels to enable accurate demodulation with reduced phase error. Compared with 2-channel implementations, the 3-channel differential architecture inherently suppresses 3rd-order harmonics and improves the signal-to-noise ratio (SNR) through inter-channel correlation. A 200-kHz Bessel filter is used to maintain constant group delay for real-time response, and a passive current-mode mixer improves linearity without incurring additional power dissipation. Fabricated in a 0.18-μm BCD technology, the prototype achieves 0.072° angular error and 1.48-μs system latency within a 20-kHz bandwidth, consuming 9.12 mA from a 5-V supply. These demonstrate state-of-the-art accuracy, the lowest reported system latency, and competitive power efficiency among IAPS interfaces.**

Keywords—inductive, angular position sensor, low latency, harmonic suppression, constant group delay.

I. Introduction

High-performance angular position sensors are essential in applications requiring precise motion control and real-time position feedback, such as electric vehicles, robotics, and medical devices. These applications impose stringent requirements on both the sensor and its readout circuitry, including robustness under harsh industrial conditions (e.g., EMI, oil contamination, humidity), tolerance to stator–rotor eccentricity that induces harmonic distortion, and minimal, predictable latency to ensure reliable operation during rapid acceleration. In addition, wide signal bandwidth is required to accurately track fast-moving or vibrating targets, while energy-efficient readout circuit design helps reduce power consumption and thermal dissipation in space- and power-constrained systems. As a result, angular position sensors and their interface circuits must achieve high accuracy, strong robustness, and low-latency operation under dynamic motion conditions.

Conventional angular position sensing techniques exhibit inherent limitations in meeting these stringent requirements. Hall-effect magnetic encoders provide low cost and CMOS compatibility; however, they require magnetic shielding and remain susceptible to demagnetization at high temperatures or over long-term operation, which degrades reliability and constrains bandwidth under fast dynamic motion. Optical encoders can achieve high accuracy but suffer from high cost, sensitivity to contamination and humidity, and long-term degradation of optical components. They also exhibit relatively high power and may introduce additional latency in real-time operation. Besides, neither technique inherently suppresses harmonic distortion, making measurement error mitigation dependent on additional power consumption and complex digital calibration.

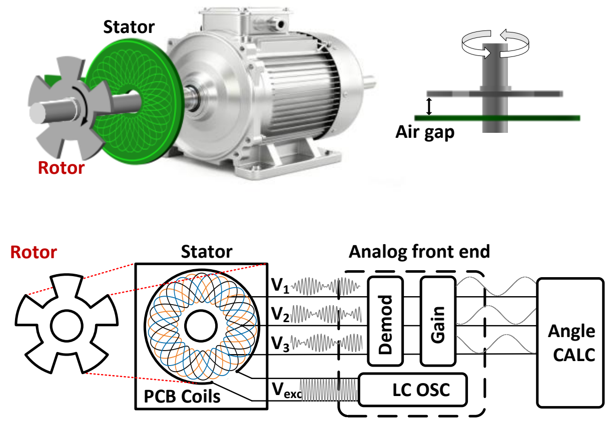

Fig. 1 Operational principles and interface architecture of a 3-channel IAPS.

Inductive sensors [1]-[4], in contrast, feature a simple structure and show strong resilience to EMI and temperature variations. As illustrated in Fig. 1, rotor motion modulates the magnetic coupling between the stator and the coils, generating three amplitude-modulated (AM) voltages with 120° phase shifts, whose amplitudes vary periodically with the rotor angle. The sense accuracy can be further improved by increasing the number of rotor pole pairs and optimizing the RX-coil layout, as shown in Fig. 5. However, as the pole count increases, the sensor becomes more susceptible to harmonic distortion [5]-[9] due to inevitable manufacturing and assembly imperfections, thus motivating the need for improved readout architectures and harmonic compensation techniques.

This work shows a 3-channel inductive angular-position sensor (IAPS) interface that fully integrates both TX and RX paths with phase-compensated clocking for accurate demodulation (Fig. 1). A low-noise on-chip LC oscillator (Fig. 2) drives the TX coil [10] (Fig. 5), while three RX coils spaced 120° apart enable differential amplification of all pairwise signal combinations. This architecture suppresses 3rd-order harmonics by 28 dB, improving angular accuracy by 38% compared to a conventional two-coil setup. Parallel signal processing across three RX channels, each followed by a 200 kHz 3rd-order Bessel filter with fixed group delay, enables accurate and low-latency angle tracking under nonuniform rotational motion. Overall, the complete IAPS interface achieves 0.072° angular error and 1.48 μs latency over a 20-kHz bandwidth while consuming 9.12 mA from a 5-V supply, including 2 mA for the LC oscillator.

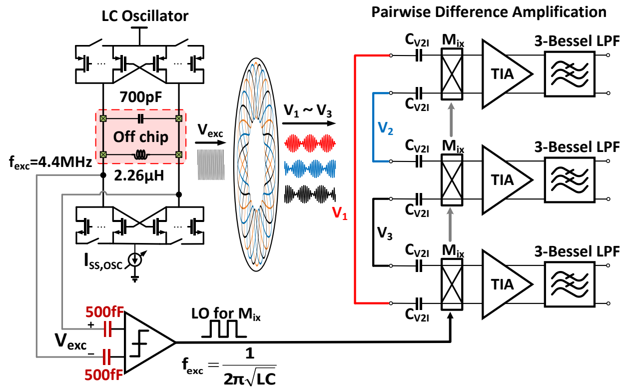

Fig. 2 Architecture of the proposed 3-channel inductive angular position sensor, including the TX and RX circuits.

II. System Architecture

A. Architecture of the IAPS Interface

The architecture of proposed 3-channel IAPS interface is shown in Fig. 2. A CMOS cross-coupled LC oscillator is employed, where the TX coil (stator) serves as the inductor element. Electromagnetic coupling between the stator and rotor induces three AM signals, V_1, V_2, and V_3, in RX coils, whose amplitudes encodes the rotor position with envelopes phase-shifted by 120°. As described by (1)–(3), differential amplification theoretically cancels the 3rd-order harmonic components. The AM signals are first converted to currents through AC-coupling capacitors (C_{V2I}) and subsequently demodulated by a passive mixer connected to the virtual ground of a transimpedance amplifier (TIA) [11-14]. The C_{V2I} capacitors block input DC components, allowing the switch transistor to process only the AC current and thereby mitigating mixer flicker noise. This configuration extracts the signal envelopes, prevents DC offsets from saturating the TIA, and preserves precise demodulation timing. The demodulated signals are then filtered by a 3rd-order Bessel filter and digitized for angle computation using a CORDIC algorithm. To achieve low latency, the filter bandwidth is set to 200 kHz, which increases the output thermal noise. This noise is mitigated by differentiating the three-phase demodulated currents prior to filtering, which both enhances the SNR and suppresses the third-order harmonic.

$$V_1 - V_2 = V_{exc}\sum_{i=0}^{\infty}\left[cos(i\omega t) - cos\left(i\omega t + i\frac{2\pi}{3}\right)\right] \quad (1)$$

$$V_2 - V_3 = V_{exc}\sum_{i=0}^{\infty}\left[cos\left(i\omega t + i\frac{2\pi}{3}\right) - cos\left(i\omega t - i\frac{2\pi}{3}\right)\right] \quad (2)$$

$$V_3 - V_1 = V_{exc}\sum_{i=0}^{\infty}\left[cos\left(i\omega t - i\frac{2\pi}{3}\right) - cos(i\omega t)\right] \quad (3)$$

B. Sensor Signal Transmission and Pathways

Fig. 3-5 show the detailed implementation of the readout circuit. The core OTA in the TIA adopts a two-stage Miller-compensated structure, providing > 90 dB DC gain and > 200 MHz gain-bandwidth product (GBW). This minimizes virtual-ground errors over the closed-loop bandwidth and reduces voltage-to-current conversion errors through the coupling capacitors C_{V2I}. The OTA is chopped to mitigate flicker noise and preserve angle resolution. The chopping clock is synchronized with the excitation signal V_{exc} to avoid aliasing of the excitation tone and its harmonics into the filter passband. Furthermore, chopping is performed at

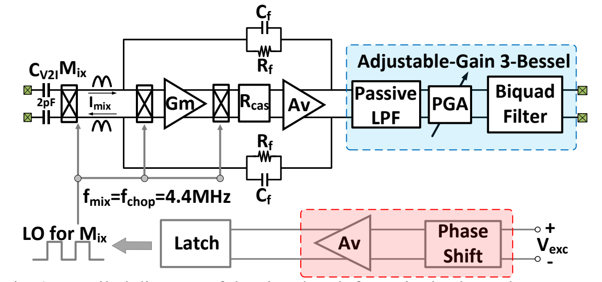

Fig. 3. Detailed diagram of the signal path for a single channel.

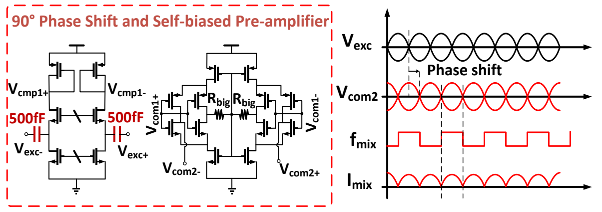

Fig. 4 Phase-shift comparator and operating principle of a sensor channel.

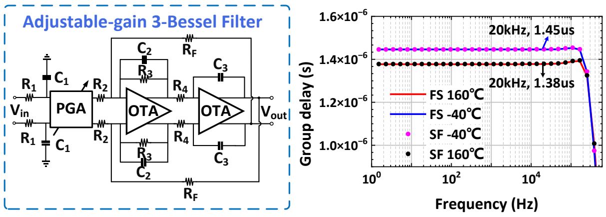

Fig. 5 Third-order Bessel filter and its response variation across corners.

the TIA virtual ground, which significantly suppresses the charge injection.

The 90° phase shift introduced by C_{V2I} requires the excitation carrier signal V_{exc} to drive a continuous-time current comparator with a pair of matched capacitors (Fig. 4), which generates a demodulation clock with accurate phase compensation [15]. At 4.4-MHz excitation frequency, the ~8 ns delay introduced by the self-biased comparator results in less than 5% signal attenuation, ensuring minimal degradation in angular resolution.

The analog-path delay, which is important for real-time angle calculation, is dominated by the low-pass filter (LPF) (Fig. 5). In practical installation, the input signal amplitude depends on the stator-rotor coupling area and separation. To mitigate delay variation caused by gain changes (0-18 dB), a programmable-gain amplifier (PGA) is inserted between the RC filter and the biquadratic filter. The delay variation of the 3rd-order adjustable-gain Bessel filter across process and temperature variations is limited to 1.38-1.45 μs within a 20-kHz bandwidth, confirming robust timing performance.

C. Mutual Coupling Principle of 5-Pole-Pair Coils

Fig. 6 illustrates the front-end coil design and assembly scheme for the IAPS. A counterclockwise excitation current I_{exc} flowing through the TX coil generates a perpendicular magnetic field B_{exc}. Through electromagnetic induction, B_{exc} induces both clockwise and counterclockwise currents in the RX coil, which cancel at nodes A and B due to the symmetric winding geometry. This configuration provides intrinsic immunity to external magnetic fields, eliminating the need for an additional magnetic shield.

The excitation field B_{exc} also introduces eddy currents in each arched segment of the rotor, thus producing secondary magnetic fields. As shown in Fig. 6 (bottom), the secondary

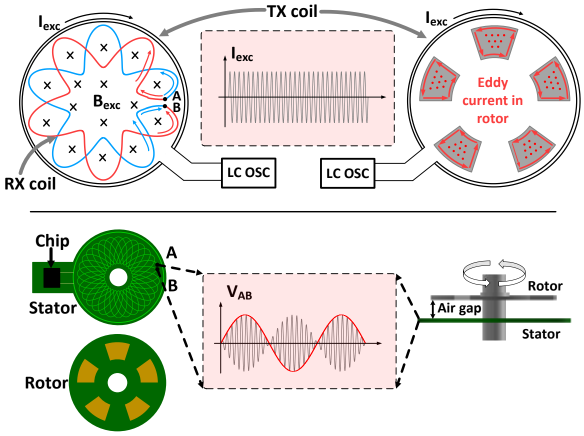

Fig. 6 Architecture and PCB layout of a 5-pole inductive sensor..

fields interact with the five-pole pairs, generating a periodic AM signal V_{AB}. The AM signal amplitude can be increased by enlarging the coil area or reducing the air gap between the rotor and stator. Within the operational range, variations in the stator-rotor distance primarily affect while preserving the linearity of the angle encoding.

III. Measurement Results

The proposed IAPS interface (Fig. 7) is implemented in a 0.18-µm, 5-V BCD CMOS process for automotive-grade compatibility, occupying 2.07 mm^2. During measurement, the rotor is mounted on a motorized stage (Fig. 8), while the PCB containing the stator and chip is fixed on a test platform. Center alignment is performed using a cursor, and the motor controls both the rotor speed and rotor-stator distance to maintain an output signal amplitude of 100 mV. The three-phase outputs from the RX coils are converted to quadrature components using Clarke transformation. After offset and gain error compensation through least-squares calibration, the rotor angle is computed by using a standard CORDIC algorithm. Note that all calibration and angle computation are implemented with conventional signal processing.

Fig. 9 compares the measured angle error between the 2-channel and 3-channel configurations. In the left plot, the 3-channel interface achieves a peak-to-peak error of 0.072° compared with the optical encoder in Fig. 8, whereas the 2-channel implementation exhibits an additional deviation of 0.072°. This result confirms the improved linearity provided by the 3-channel architecture. It should be noted that both configurations utilize identical calibration and computation procedures. The proposed interface maintains its accuracy across a wide temperature range from -40 °C to 160 °C. The slight degradation observed at high temperatures is mainly attributed to the reduced oscillator excitation amplitude, which can be mitigated by increasing the programmable tail current. Furthermore, the embedded PGA constrains the input overdrive, preventing saturation and ensuring robust operation.

Fig. 10 shows the measured filter bandwidth and group delay, along with the angle resolution across ten samples. As shown in Fig. 11, the measured system latency is 1.48 µs, enabled by the implementation of a 200-kHz 3rd-order filter.

Fig. 12 compares the 3rd-harmonic rejection between the 2- and 3-channel readouts. The 3-channel design achieves a 28.13dB improvement in suppression, demonstrating its excellent linearity.

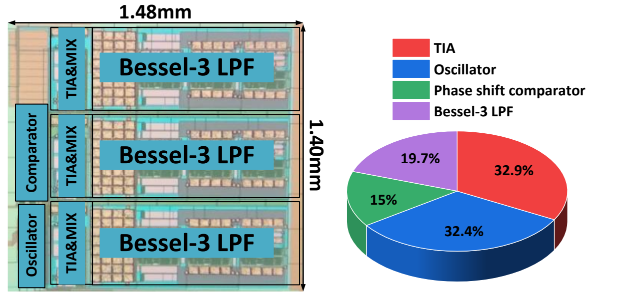

Fig. 7 Die micrograph and measurement setup of the IAPS interface.

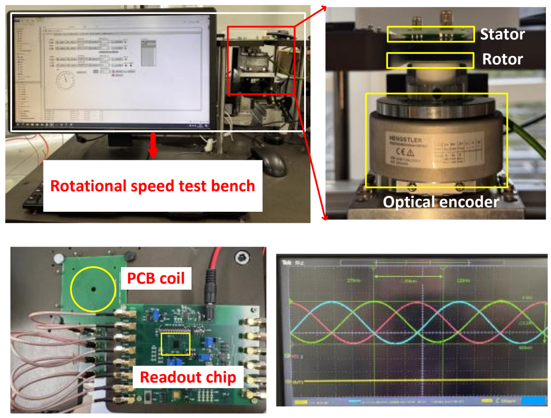

Fig. 8 Measurement setup for the IAPS interface.

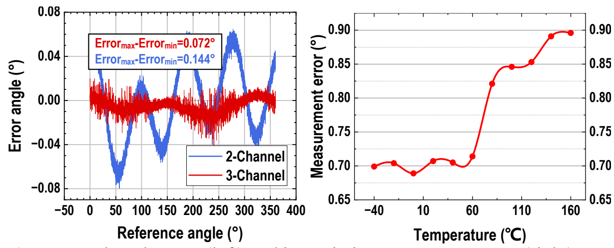

Fig. 9 Measured angle error (left) and its variation over temperature (right).

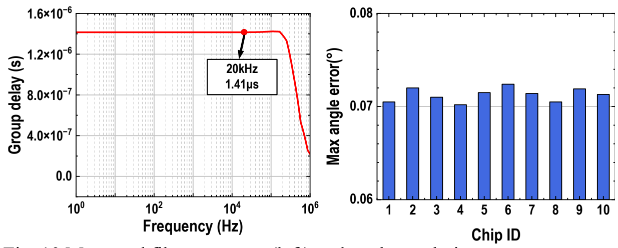

Fig. 10 Measured filter response (left) and angle resolution across ten samples (right).

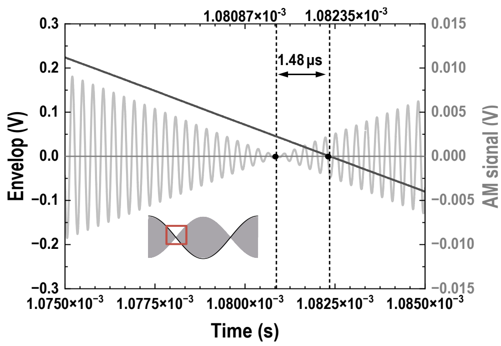

Fig. 11 Measured system latency.

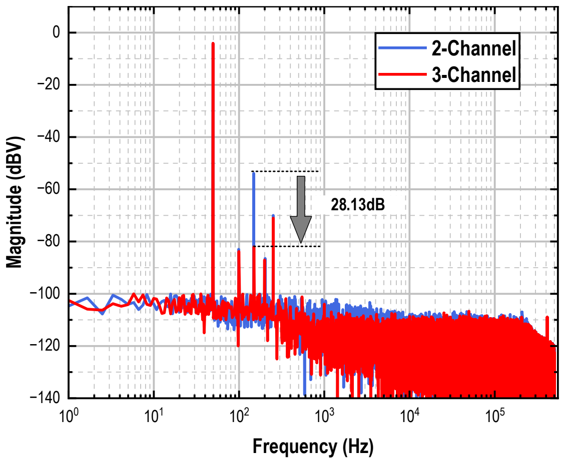

Fig. 12 Third-harmonic suppression comparison of the 2- and 3-channel readout interfaces.

Table I compares the proposed IAPS interface circuit with state-of-the-art solutions. The 3-channel architecture effectively suppresses harmonic distortion, achieving a constant system delay of 1.48 µs, a peak-to-peak angle error of 0.072°, and a bandwidth of 20 kHz. This accuracy is obtained using conventional low-power calibration and computation, in contrast to [9], which relies on complex and power-intensive signal processing schemes. Furthermore, while the displacement sensor in [1] achieves high precision by reducing the measurement range, such an approach is inherently unsuitable for angle sensing. Implemented in a 0.18 µm, 5 V automotive CMOS process, the proposed 3-channel interface consumes a total current of only 9.12 mA and achieves a best-in-class energy efficiency with an FoM of 132.1 dB.

TABLE I. PERFORMANCE COMPARISON WITH STATE-OF-THE-ART

		This work	MLX90510 [5]	AS5715R [6]	NCV77320 [7]	IPS2550 [8]	NCS32100 [9]
Technology (nm)		**180**	-	-	-	-	-
Current (mA)		**9.12**	16~20	10~15	11~12.5	8~32	82~133
No. of channels		**3**	3	2	2	2	2
Bandwidth (Hz)		**20k**	4k	8k	-	10k	100/1k*1
System delay (µs)		**1.48**	-	3.3~5.8	-	3.8~4.2	7
Angle error	(°)	**0.072**	-	0.075	0.54	0.36	0.014*5
	(° el.)*2	**0.36**	0.36	-	-	-	-
Resolution (bit)		**12.28**	12.28	12.23	9.38	9.96	14.66
FoM (dB)*3		**132.1**	122.6*4	126.4*4	-	113.2*4	113.4*4

*1 Accuracy degrades at 1kHz bandwidth;
*2 1° mechanical =N° electrical, where N denotes the number of pole pairs;
*3 Resolution is calculated over 360°, and FoM = DR+10$\log_{10}$(BW/Power);
*4 FoM calculated using the typical power consumption.
*5 With complex and power-intensive signal-processing schemes.

CONCLUSION

This work presents a 3-channel inductive angular-position sensor (IAPS) interface achieving high linearity, low latency, and strong noise immunity for high-speed precision sensing. The 3-channel differential architecture suppresses 3rd-harmonic distortion and improves the SNR, while a wideband 3rd-order Bessel filter provides a constant group delay. By further combining passive current-mixing demodulation with a low-noise TIA, the proposed design achieves low latency and high accuracy among reported IAPS interfaces, making it suitable for robust and energy-efficient automotive angle sensing.

ACKNOWLEDGMENT

This work was supported by the State Key Laboratory of Integrated Chips and Systems (SKL-ICS), and Jiashan-Fudan Institute, Jiashan 314102, China.

REFERENCES

[1] V. Chaturvedi, M. R. Nabavi, J. Vogel, K. A. A. Makinwa, and S. Nihtianov, “A 0.6nm resolution 19.8mW eddy-current displacement sensor interface with 126MHz excitation,” *ISSCC*, pp. 174–175, Feb. 2017.

[2] M. R. Nabavi, M. A. P. Pertijs and S. Nihtianov, “An interface for eddy-current displacement sensors with 15-bit resolution and 20 MHz excitation,” *IEEE JSSC*, vol. 48, pp. 2868–2881, Nov. 2013.

[3] M. Oberle, R. Reutemann, R. Hertle and Q. Huang, “A 10-mW two channel fully integrated system-on-chip for eddy-current position sensing [in biomedical devices],” *IEEE JSSC*, vol. 37, pp. 916–925, July 2002.

[4] S. Xia, K. Makinwa and S. Nihtianov, "A capacitance-to-digital converter for displacement sensing with 17b resolution and 20µs conversion time," *ISSCC*, pp. 198-199, Feb. 2012.

[5] Melexis, “MLX90510 high-speed inductive position sensor,” Datasheet, 2022.

[6] Ams OSRAM, “AS5715R on-/off-axis inductive position sensor with sin/cos output,” Datasheet, 2021.

[7] onsemi, “Inductive position sensor interface NCV77320,” Datasheet, 2022.

[8] Renesas, “Inductive position sensor IC IPS2550,” Datasheet, 2022.

[9] onsemi, “Inductive position sensor with battery backup NCS32100,” Datasheet, 2022.

[10] A. Hajimiri and T. H. Lee, “Design issues in CMOS differential LC oscillators,” *IEEE JSSC*, vol. 34, pp. 717–724, May 1999.

[11] P. G. R. Silva, L. J. Breems, K. A. A. Makinwa, R. Roovers, and J. H. Huijsing, “An IF-to-baseband modulator for AM/FM/IBOC radio receivers with a 118 dB dynamic range,” *IEEE JSSC*, vol. 42, pp. 1076–1089, May 2007.

[12] W. Redman-White and D. M. W. Leenaerts, “1/f noise in passive CMOS mixers for low and zero IF integrated receivers,” *ESSCIRC*, pp. 41–44 Sep. 2001.

[13] Q. Fan, F. Sebastiano, J. H. Huijsing, and K. A. A. Makinwa, “A 1.8 µW 60 nV /√H z capacitively-coupled chopper instrumentation amplifier in 65 nm CMOS for wireless sensor nodes,” *IEEE JSSC*, vol. 46, pp. 1534‑1543, Jul. 2011.

[14] S. Chehrazi, A. Mirzaei, and A. A. Abidi, “Noise in current-commutating passive FET mixers,” *IEEE Trans. Circuits Syst. I, Reg. Papers*, vol. 57, pp. 332–344, Feb. 2010.

[15] V. Milovanovic and H. Zimmermann, “A 40 nm LP CMOS self-biased continuous-time comparator with sub-100ps delay at 1.1V & 1.2mW,” *ESSCIRC*, pp. 101–104, Sep. 2013.